NASA TECHNICAL NOTE

NASA TN D-8068

NASA TN D-8068

A COMPARISON OF MEASURED AND PREDICTED TEST FLOW IN AN EXPANSION TUBE WITH AIR AND OXYGEN TEST GASES

Kenneth V. Haggard and William K. Goad

Langley Research Center
Hampton, Va. 23665

NATIONAL AERONAUTICS AND SPACE ADMINISTRATION • WASHINGTON, D. C. • DECEMBER 1975

1 Report No	2. Government Accession No.	3. Recipient's Catalog No.
NASA TN D-8068		

4. Title and Subtitle
A COMPARISON OF MEASURED AND PREDICTED TEST FLOW IN AN EXPANSION TUBE WITH AIR AND OXYGEN TEST GASES

5. Report Date
December 1975

6. Performing Organization Code

7. Author(s)
Kenneth V. Haggard and William K. Goad

8. Performing Organization Report No.
L-10356

9. Performing Organization Name and Address
NASA Langley Research Center
Hampton, Va. 23665

10. Work Unit No.
176-24-31-01

11. Contract or Grant No.

12. Sponsoring Agency Name and Address
National Aeronautics and Space Administration
Washington, D.C. 20546

13. Type of Report and Period Covered
Technical Note

14. Sponsoring Agency Code

15. Supplementary Notes

16 Abstract

Simultaneous time-resolved measurements of temperature, density, pitot pressure, and wall pressure in both air and O_2 test gases have been obtained in the Langley pilot model expansion tube. These tests show nonequilibrium chemical and vibrational relaxation significantly affect the test-flow condition. The use of an electromagnetic device to preopen the secondary diaphragm before the arrival of the primary shock wave resulted in an improvement in the agreement between the measured pitot pressure and the value inferred from measured density and interface velocity. Boundary-layer splitter plates used to reduce the wall boundary layer have shown that this disagreement in the measured and inferred pitot pressures is not, as speculated in NASA TN D-7273, a result of boundary-layer effects.

17. Key Words (Suggested by Author(s))	18. Distribution Statement
Expansion tube Vibrational temperatures	Unclassified – Unlimited Subject Category 34

19. Security Classif. (of this report)	20. Security Classif. (of this page)	21. No. of Pages	22. Price*
Unclassified	Unclassified	34	$3.75

*For sale by the National Technical Information Service, Springfield, Virginia 22161

A COMPARISON OF MEASURED AND PREDICTED TEST FLOW IN AN EXPANSION TUBE WITH AIR AND OXYGEN TEST GASES

Kenneth V. Haggard and William K. Goad
Langley Research Center

SUMMARY

Simultaneous time-resolved measurements of temperature, density, pitot pressure, and wall pressure in both air and O_2 test gases have been obtained in the Langley pilot model expansion tube. These tests show nonequilibrium chemical and vibrational relaxation significantly affect the test-flow condition. The use of an electromagnetic device to preopen the secondary diaphragm before the arrival of the primary shock wave resulted in an improvement in the agreement between the measured pitot pressure and the value inferred from measured density and interface velocity. Boundary-layer splitter plates used to reduce the wall boundary layer have shown that this disagreement in the measured and inferred pitot pressures is not, as speculated in NASA TN D-7273, a result of boundary-layer effects.

INTRODUCTION

For several years a research program has been conducted at Langley Research Center to determine a range of operating conditions for which the expansion tube flow is suitable for hypervelocity testing. Experimental studies performed in the Langley pilot model expansion tube are described in references 1 to 4, and several idealized theoretical flow models are described in references 5 to 10. The complexity of the expansion tube flow cycle is such that, in spite of this extensive long-term effort, it has not been possible to develop a flow model that can consistently predict the test-flow conditions or explain the relationships between the measured test-flow quantities.

The study described in reference 1 used simultaneous measurements of wall pressure, pitot pressure, O_2 density, and the vibrational temperature of O_2 to demonstrate that chemical and vibrational nonequilibrium processes were probably important in the flow cycle. These results are in qualitative agreement with the predictions of references 8, 9, and 10. However, the temperature and density measurements were dependent on absorption measurements made across the tube diameter and were thus influenced by the wall boundary layer. Self-consistency checks among the four measurements and estimates of the wall boundary-layer thickness obtained from reference 4 indicated there could be an error of as much as 20 percent in the measured density due to the boundary layer.

The present study was undertaken to determine the effects of nonequilibrium chemical and vibrational relaxation on an expansion tube test flow. These tests were conducted with both pure O_2 and air as a test gas, and the range of test conditions was extended beyond that of reference 1 to better determine the appropriate flow model for the facility. These studies used a set of splitter plates in the test section to reduce the effects of the wall boundary layer on the density and temperature measurements.

Some experiments used an electromagnetic device to open the secondary diaphragm prior to the arrival of the shock wave. This device could conceivably improve the quality of the test flow by reducing the contamination from the diaphragm material and by eliminating the need for the test flow to supply the momentum necessary to open the diaphragm.

SYMBOLS

A_λ	absorption parameter
a	sound speed, m/s
F	mass fraction of O_2
H	enthalpy, m^2/s^2
I_λ	intensity at λ (arbitrary units)
$I_{\lambda,o}$	unabsorbed intensity at λ (arbitrary units)
k_λ	absorption coefficient at λ, cm^{-1}
L	distance from secondary diaphragm to test section, m
l	length, cm
M	molecular weight of initial test gas
p	pressure, Pa
p_t	pitot pressure, Pa
$p_{t,c}$	pitot pressure defined by equation (9), Pa

p_w	wall pressure, Pa
R	universal gas constant, 8.31 J/mole-K
T	temperature, K
T_{v,O_2}	vibrational temperature of O_2, K
t	time
t_5	time after arrival of test flow at test section, s
t_{res}	residence time of fluid particle behind primary shock, s
V	flow speed, m/s
V_i	speed of secondary interface, m/s
$V_{S,1}$	speed of primary shock wave, km/s
x	distance, m
Z	compressibility factor
α	ratio defined in equation (3)
Δ	$= \frac{p_{t,c}}{p_t}$
λ	wavelength, nm
ρ	density, kg/m^3
ρ_d	scale depth, cm (see eq. (5))
ρ_{O_2}	density of O_2, kg/m^3

Subscripts:

0	standard conditions (0.101325 MPa; 273.3 K)
1	initial state in intermediate section
2	state behind primary shock
5	state of test-gas flow
6	state behind reflected shock at secondary diaphragm
10	initial state in acceleration section

DESCRIPTION OF FACILITY

The Langley pilot model expansion tube was a pilot facility designed to study the feasibility of using an expansion tube to produce a short duration hypersonic flow duplicating conditions encountered by an entry vehicle. This pilot model facility was terminated when the Langley 6-inch expansion tube at Langley Research Center became operational (see ref. 11). The pilot model tube was a 9.55-cm-diameter stainless steel tube consisting of three sections: a driver section 1.55 m long, a 10-m intermediate section, and a 9.75-m acceleration section. The driver and intermediate sections were separated by a 3.17-mm-thick steel diaphragm. The intermediate and acceleration sections were separated by either a 0.00635-mm Mylar diaphragm or a 0.4-mm-thick aluminum sheet.

An idealized distance-time diagram of the flow cycle is shown in figure 1(a). In order to start the cycle, the intermediate chamber was filled with the test gas (state ①) and the acceleration section was filled with helium (state ⑩). The driver section was then pressurized with hydrogen (state ④) until the first diaphragm ruptured. At this time the primary shock wave was formed; as the shock wave moved down the intermediate section, it compressed and heated the test gas to state ②. The shock was reflected when it reached the Mylar diaphragm, and the increased pressure caused the diaphragm to rupture. The details of this process are shown in figure 1(b), where it has been assumed that the diaphragm opens instantaneously a short time after the shock reflection. A secondary shock wave is formed and moves down the acceleration section when the Mylar diaphragm ruptures, and a second expansion fan provides the transition from the reflected shock region (state ⑥) to the final

test flow (state ⑤). For the conditions at which these tests were made, the test flow is ended by the arrival of the tail of the expansion fan at the test section.

INSTRUMENTATION

The instrumentation used to measure pressure and wave speeds is described in references 1 and 2. The speed of the shock waves was measured by using a combination of pressure transducers, ion gaps, and microwave reflection. The interface speed was usually determined by microwave reflection with a back up of photodetectors and pitot pressure measurements. A description of the microwave reflection technique is contained in reference 12.

A sketch of the arrangement of the equipment used to measure density and temperature at the test section is shown in figure 2(a). The ultraviolet source has a capillary tube through which hydrogen was continuously pumped. An artificial transmission line was connected across the lamp and a spark series gap. A synchronized pulse triggered by the primary shock breaks down the spark gap so that the artificial transmission line discharges through the lamp, thereby producing an intense source of vacuum ultraviolet radiation that lasts for more than 2 ms. The light from the lamp passes through the test section of the tube via two CaF_2 windows and into a 0.5-m vacuum ultraviolet spectrograph. The intensity of the diffracted beam was measured at 147 and 160 nm over a bandwidth of 0.8 nm by sodium salicylate coated 1P21 photomultiplier tubes. The output of each phototube was displayed on an oscilloscope and photographed.

A sketch of the test section with the splitter plates in position is shown in figure 2(b). The plates were 36.5 mm wide and 53 mm long, with the window 25 mm behind the leading edge. The plates were spaced 27 mm apart. Wall pressure was measured just upstream of the light beam, and the pitot pressure was measured just downstream of the beam and on the center line of the tube. For the conditions investigated, the splitter plates did not affect the pitot pressure measured by the probe during that part of the flow covered by these studies.

It is estimated that there is typically a ±20-percent error in the temperature measurement and a ±10-percent error in the density and pressure measurements.

DIAPHRAGM OPENER

The secondary diaphragm is generally opened by the increase in pressure behind the reflected shock in the test gas. Thus the diaphragm is subjected to the high temperatures of the reflected shock region; and although the exposure time is short – a few microseconds – surface contamination on the diaphragm is transferred to the test gas. In addition, the test gas loses momentum to the diaphragm during the opening process. In an attempt to reduce

these problems without introducing other major detrimental effects, an electromagnetic device was used to open the diaphragm prior to the arrival of the primary shock wave.

A sketch of the diaphragm-opener coil is shown in figure 3. It consisted of an insulated aluminum coil with an inner diameter of 9.55 cm and an outer diameter of 14.68 cm. The two parallel plate prongs served to connect the coil to a high voltage capacitor bank. The installation of the coil in the expansion tube is shown in figure 4. The prongs extended out of the tube through a double O-ring seal, and the body of the coil was supported inside the tube by a fiberglass liner. Upstream of the diaphragm location, the inner diameter of the liner matched that of the tube; however, downstream of the diaphragm location, the inner diameter opened up to the outer diameter of the coil and then tapered down to the tube diameter. No studies were made of the effects on the flow of the area change in the tube downstream of the coil. A 0.4-mm-thick aluminum sheet was used as a diaphragm. The center of the diaphragm was scribed with a cross to half thickness, and the diaphragm was clamped into position so that it made contact with the downstream side of the coil.

When the capacitor bank was discharged through the coil, the electromagnetic field about the coil generated eddy currents in the diaphragm; consequently, the diaphragm was forced away from the coil, causing it to tear along the scribes. Once the tabs had been given the initial momentum, the fact that they were clamped at the outer edge caused them to swing outward into the enlarged area just downstream of the coil where they were out of the direct flow. So long as an excessive amount of energy was not transferred to the diaphragm, the tabs did not tear loose and the opened tabs remained in the enlarged area throughout the rest of the flow cycle.

A series of photographs of the opening process is shown in figure 5. These photographs were taken during a bench test of the opener. The bank voltage was 5.3 kV and the energy was 10.8 kJ. The first photograph (fig. 5(a)) shows the initial tearing of the diaphragm along the scribes. At this time the diaphragm is still conducting a large eddy current, and the sudden tearing of the diaphragm causes the arcing across the tears between the tabs. The second and third photographs (figs. 5(b) and (c)) were taken at 10-μs intervals and show the arcing peak and start to diminish. The other photographs show the continued opening of the tabs.

For a large number of bench tests and for eight expansion tube tests, the diaphragm opener performed well mechanically. However, on the ninth expansion tube test, the trigger signal failed to discharge the bank and the diaphragm was forced open by the reflected shock wave. The coil seemed to have survived this trouble with no damage; however, on the next test the insulation on the coil broke down and the coil was shorted. This breakdown

destroyed the coil and ended the testing with the opener. The authors feel it is probable that the coil insulation had been damaged in the eighth run since the insulation had withstood repeated bench tests under voltages as high as 8 kV.

Because of the limitations in the facility, it was not possible to install the microwave measurement device in the tube with the diaphragm opener in use. Thus, the interface velocities for these runs were obtained from phototube records and the pitot pressure measurements. Although no tabs were torn off during these tests, the possibility was such a constant worry that the splitter plates were removed from the tube during the diaphragm-opener runs.

DATA REDUCTION

The vibrational temperature and density of O_2 were determined from the absorption measurements by using the method described in references 13 and 14. Basic data and a theoretical treatment are to be found in references 15 and 16. With this technique the transmission of the flow is measured at two wavelengths (147 and 160 nm). These wavelengths were selected because the absorption coefficient at 147 nm is sensitive to temperature whereas the absorption coefficient at 160 nm is relatively insensitive to temperature. Thus, since the absorption is only a function of temperature, density, and wavelength, the temperature and density can be determined. This procedure will become clear by considering the equations governing the absorption process.

The attenuation of the ultraviolet radiation was assumed to follow Beer's law. Thus,

$$I_\lambda(t) = I_{\lambda,o}(t)\exp\left[-\frac{1}{\rho_0}\int \rho(t)k_\lambda(t)\,dl\right] \tag{1}$$

where ρ_0 is the absorber density $\left(O_2 \text{ in this case}\right)$ and the integral is taken over the absorption path. The absorption parameter A_λ is defined by the relation

$$A_\lambda(t) = \log_e\left[\frac{I_{\lambda,o}(t)}{I_\lambda(t)}\right] = \frac{1}{\rho_0}\int \rho(t)k_\lambda(t)\,dl \tag{2}$$

and α, the ratio of A_{147} to A_{160}, is

$$\alpha(t) = \frac{A_{147}(t)}{A_{160}(t)} = \frac{\int \rho(t)k_{147}(t)\,dl}{\int \rho(t)k_{160}(t)\,dl} \tag{3}$$

where the subscripts 147 and 160 are values of λ in nanometers.

The data-reduction model for the density and vibrational temperature of O_2 includes the following three assumptions:

(1) A valid vibrational temperature exists in the flow (i.e., the vibrational energy levels have a Boltzmann distribution)

(2) Absorption by species other than O_2 is negligible

(3) Flow quantities are uniform along the absorption path.

With these assumptions, α becomes

$$\alpha(t) = \frac{k_{147}(t)}{k_{160}(t)} \tag{4}$$

Plots of k_{147}, k_{160}, and α as a function of temperature are shown in figure 6. These curves have been taken from reference 14.

Once α is obtained from measured values of A_λ, T_{v,O_2} can be found from figure 6. The scale depth ρ_d is defined by

$$\rho_d(t) \equiv \int \frac{\rho(t)}{\rho_0} \, dl = \frac{A_\lambda(t)}{k_\lambda(t)} \tag{5}$$

The O_2 density is then obtained from

$$\rho_{O_2}(t) = \frac{\rho_{O_2,0}}{l} \rho_d(t) \tag{6}$$

where l is the path length across the flow.

When each of the values p_w, p_t, ρ_{O_2}, T_{v,O_2}, and V_i have been measured, they can be cross-checked by using the equation of state and by assuming that the flow is in thermodynamic equilibrium. The flow density is then obtained from

$$\rho(t) = \frac{1}{F} \rho_{O_2}(t) \tag{7}$$

where the mass fraction F of O_2 in the flow can be calculated from the measured pressure and temperature. Thus, the values of each measured quantity can be compared with the value obtained from the other measured quantities and from the relation

$$p = \frac{Z\rho RT}{M} \tag{8}$$

where Z is assumed to be unity. If, in addition, it is assumed that the flow velocity is given by the interface velocity, then the pitot pressure is approximately given by

$$p_{t,c} = \rho V_i^2 \tag{9}$$

This relation (eq. (9)) is accurate to within 3 percent for the conditions tested and is valid even if the flow is not in thermodynamic equilibrium. Thus, if Δ is defined as

$$\Delta \equiv \frac{p_{t,c}}{p_t} = \frac{\rho_{O_2} V_i^2}{F p_t} \tag{10}$$

and is set equal to unity, the mass fraction of O_2 in the flow can be found from

$$F = \frac{\rho_{O_2} V_i^2}{p_t} \tag{11}$$

When a value of Δ is given, it has been obtained by assuming that F is defined by its value in the initial test gas (state ①, fig. 1).

A detailed discussion of the measurement errors in the vibrational temperature is given in reference 1. In general, errors of 20 percent in T_{v,O_2} and 10 percent in density and pressure are expected. Measurements of the shock and interface speeds are accurate to 1 or 2 percent.

THEORETICAL FLOW MODELS

Wave diagrams similar to those in figure 1 can be used to construct mathematical models of the expansion tube flow cycle (see, for example, refs. 5 to 10). Because of the complex nature of the expansion tube flow, each of these models involves major simplifying assumptions. For example, they all neglect viscous effects and interface mixing. The model described in reference 7 treats the finite opening time of the secondary diaphragm, and the models

described in references 8 to 10 treat finite-rate chemical and vibrational relaxation in part of the flow cycle.

There are five flow models that seem to provide good upper and lower bounds for the measured flow quantities. These models (ISPG, ISEE, RSEE, ISFE, and RSFE) are described as follows and are discussed in more detail in references 1 and 17: The ISPG model assumes the test gas is a perfect gas. The flow quantities are calculated by using the flow diagram in figure 1(a) (no reflected shock); the expansion process is assumed to be isentropic. The ISEE model, like the ISPG model, assumes there is no reflected shock at the secondary diaphragm and that the expansion process is isentropic. However, the test gas is assumed to be real, and the equilibrium properties of the fluid are used throughout the flow cycle. The RSEE model assumes there is a reflected shock upstream of the secondary diaphragm and that the entire test flow is processed by this shock. The expansion is assumed to be isentropic, and equilibrium flow properties are used throughout the entire calculation. This RSEE model neglects any effects of the interaction of the head of the expansion fan with the reflected shock. The ISFE and RSFE models are similar to the ISEE and RSEE models except that the ISFE and RSFE models assume the flow becomes frozen upon entering the expansion fan. That is, the chemical composition and vibrational energy are fixed at the equilibrium values just upstream of the head of the expansion fan, and the chemical composition and vibrational energy remain constant during the rest of the flow cycle.

These five models neglect the finite rates of chemical and vibrational relaxation; however the frozen-expansion and equilibrium-expansion processes should provide limits on this non-equilibrium problem. The only attempt to treat the nonequilibrium character of the flow theoretically is described in references 8, 9, and 10. The model described therein assumes the flow is in equilibrium until it enters the expansion fan and only then allows for finite-rate chemical and vibrational relaxation. This assumption breaks down for particle paths near the diaphragm since the flow along these paths cannot reach equilibrium before entering the expansion fan. The severity of this breakdown can be seen by examining the nonequilibrium flow behind the primary shock for a typical test condition. For such a case the mole fraction of oxygen atoms as a function of time is shown in figure 7. The test gas is pure O_2, and the shock speed is 2956 m/s, and the initial temperature is 300 K. The equilibrium mole fraction of O is calculated to be 0.115. The abscissa is the residence time t_{res} of the fluid particle between the shock into state (1) and the head of the expansion fan (this assume there is no reflected shock). By assuming that states (2) and (5) in figure 1(a) are uniform, t_{res} can be related to the test time t_5 of that fluid particle. The test time t_5 is the time after the arrival of the secondary interface at the test section. Thus

$$t_{res} = \rho_5 t_5 V_5 \left(\frac{1}{\rho_1 V_{S,1}} + \frac{1}{\rho_2 a_2} \right) \tag{12}$$

For the conditions of this test the test flow is ended by the arrival of the tail of the expansion fan at the test section. Thus the maximum test time $t_{5,max}$ is

$$t_{5,max} = L\left(\frac{1}{V_i - a_5} - \frac{1}{V_i}\right) \tag{13}$$

For this same test, the maximum residence time is 109 μs for the ISEE model but 23.5 μs for the ISFE model. These times are so marked by the circles in figure 7. Clearly, the flow does not reach equilibrium behind the primary shock; and if a nonequilibrium calculation of the flow cycle is to be undertaken, it must start with the primary shock, not with the expansion fan.

All of the calculations for the various theoretical models used in this report were made with the use of the computer code described in reference 17. The nonequilibrium data for figure 7 were obtained from the computer code of reference 18.

TEST CONDITIONS

The initial pressures, the test-gas composition, and the measured primary shock and secondary interface speeds are listed in table 1. In all cases the driver section contained hydrogen, and the acceleration section either contained helium or was evacuated. The initial test-gas pressure p_1 varied from 2933 to 333 Pa and the acceleration section pressure p_{10}, from 133 to less than 1 Pa. Primary shock speeds ranged from 4002 to 2718 m/s, and the interface velocity varied from 6458 to 4938 m/s.

RESULTS AND DISCUSSION

Time Variations

Because of the broad range of conditions tested, it is not possible to pick one condition that is representative of the entire range covered in this report; however, there is one condition that produces test results for which the measured values of p_w, p_t, ρ, T_{v,O_2}, and V_i are in good agreement with each other when equations (8) and (9) are used to compare the flow quantities. This condition is run 3676 in table 1. Time histories of an example of the run at this condition are shown in figure 8. The test gas is O_2 at an initial pressure of 2933 Pa; the primary shock speed is 2955 m/s, and the flow was expanded to 6101 m/s. The measured values of p_w, p_t, ρ, and T_{v,O_2} are denoted by the continuous curves and are plotted as a function of the test time t_5. For each flow quantity, equation (8) or (9) has been used to infer the corresponding value based on the other measured values. These

inferred values have been averaged over 25-μs intervals to reduce the scatter of the experimental data and are denoted in figure 8 by the circular symbols.

The comparison between the measured and calculated values is quite good and generally falls within the experimental error for the data. The wall pressure and density are in agreement within the experimental error. On the basis of experimental error, the pitot pressure shows somewhat more variation than is expected; this variation may be due to an increase in the flow velocity behind the interface, as reported in reference 4. The rapid increase in density and decrease in temperature early in the flow is, in part, a result of the response time (2.5 μs) of the system but may also be caused by mixing at the interface. It should be recalled that the measured temperature is a vibrational temperature and the temperature inferred from the density and wall pressure is a translational temperature; the difference between them is probably an indication of vibrational nonequilibrium.

A second example, run 3679, of the time history of the flow is shown in figure 9. The initial conditions upstream of the secondary diaphragm for this run are about the same as for the previous example; however, no helium was added in the acceleration section. Thus the flow has been expanded to a very low pressure, and there is no detectable region of uniform flow conditions. The pressure and density measurements are nearly ramp functions with time, and the vibrational temperature takes about 100 μs to come to equilibrium with the static temperature instead of the 25 μs in the previous example. This longer relaxation time is qualitatively what would be expected if the flow were not in vibrational equilibrium during the early part of the flow.

Data Trends

As a means of obtaining data trends, tests have been grouped according to test gas and shock speed, and the results are plotted as a function of V_i. Because the pressure at which the first diaphragm ruptured was not the same for each run, there is a small scatter in $V_{S,1}$ (about 1.5 percent). This effect was eliminated by plotting the conditions for an average $V_{S,1}$. In order to correct for the differences introduced between the measured and theoretical predictions by this averaging process, the measured data were scaled using the RSEE and RSFE models. Thus the location of the data relative to the RSEE and RSFE predictions is the same for both the true and the averaged test condition. This procedure is described in detail in reference 1.

The variations of ρ, T, p_w, and p_t with interface speed for a series of tests with air as a test gas are shown in figure 10. The circular and square symbols denote the averages of the measured data over a period of 50 μs in t_5 from t_5 = 50 μs to t_5 = 100 μs. The triangular symbol denotes the corresponding value inferred from equation (8) or (9). In addition, if the measured value can be determined over the first 50 μs of the flow and if it

is significantly different from the average over the second 50 μs, the range of these two averages is indicated by a bar. The predicted curves were obtained by using p_1, T_1, $V_{S,1}$, V_i and the computer code described in reference 17.

The measured densities, figure 10(a), always lie above the RSFE model and, with but two exceptions, are below the predicted value of any of the other models. The values of density inferred from equation (8), p_w, and T_{v,O_2} lie near or below the measured value and show better agreement with the measured values for the higher velocity cases. The tests made with the diaphragm opener show much better agreement between the inferred and measured values although this could be a velocity effect rather than a result of the diaphragm opener.

The variation of T_{v,O_2} is shown in figure 10(b). The theoretical predictions here refer to the translational temperature, not to the vibrational temperature. For this case the vibrational temperatures for the ISFE and RSFE models are 3169 and 4985 K, respectively. With but two exceptions the inferred temperature (obtained from eq. (8), p_w, and ρ) lies well below the measured value. This indicates that the flow is not in vibrational equilibrium.

The measured wall pressures, figure 10(c), generally fall between the ISFE and ISEE predictions. The values inferred from equation (8) are generally higher, with the best agreement between the measured and inferred values again occurring for the higher interface speeds and the diaphragm opener runs.

The measured pitot pressures, figure 10(d), show almost no systematic variation with interface speed. The values inferred from equation (9) are generally above the measured values, with the only two exceptions being two diaphragm opener tests. In general, the data lie between the frozen predictions.

The data trend as a function of interface speed for a series of tests with O_2 as the test gas is shown in figure 11. Because the accuracy of the density and temperature measurement depends on the amount of O_2 in the light beam, these tests were made at a lower density than were the air runs.

The density measurements, figure 11(a), lie about the ISFE prediction and show good agreement between the measured and inferred values. Also shown in figure 11(a) are two runs at V_i of 6250 and 6350 m/s which were made without adding any helium to the acceleration chamber and thus show large changes in the measurements since there is no period of steady flow.

The vibrational temperature, figure 11(b), shows some good agreement between the measured and inferred values for the second 50 μs average but also shows strong relaxation with time for the first 50 μs. This indicates that while the vibrational temperature is far from the translational temperature early in the flow, it is approaching equilibrium with time.

The wall pressure, figure 11(c), falls just below the ISPG model and again shows good agreement between the measured and inferred values.

The pitot pressure, figure 11(d), lies about the ISFE prediction and shows fair agreement between the measured and inferred values for most cases.

These results for air and O_2 indicate that none of the theoretical models examined provides a means of predicting the state of expansion tube test flow over the range of conditions tested. One possible explanation for this is the fact that the flow is highly sensitive to small levels of dissociation. This sensitivity is illustrated by figure 11(d). The O_2 mass fraction at the test section for the ISFE model is 0.94; thus, if the flow were described by the model, the pitot pressure inferred from equation (9) should be 6 percent less than the measured pitot pressure. However, the predicted values obtained from the ISEE and ISFE models differ by more than 250 percent.

In order to accentuate the effects of dissociation, a series of tests were made with O_2 at a reduced pressure as the test gas. This resulted in a stronger primary shock and higher degree of dissociation upstream of the expansion fan. The ratio Δ for these tests is shown in figure 12, where it has been plotted as a function of the stagnation enthalpy (calculated from ref. 17) behind the reflected shock at the secondary diaphragm. The mass fraction F has been assumed to be unity, and equation (9) has been used to calculate $p_{t,c}$; thus Δ becomes

$$\Delta = \frac{\rho_{O_2}}{\rho_{O_2} + \rho_0} \tag{14}$$

Consequently, Δ should be unity if the flow is in thermodynamic equilibrium and less than unity for any degree of nonequilibrium. Figure 12 shows Δ to be in good agreement with the RSFE model for H_6 greater than 10^7 m^2/s^2; however for H_6 less than this, the differences between the models are less than the experimental errors in Δ. The reader should not assume that figure 12 shows the RSFE model to be the proper model for these flow conditions; it only shows that to a good approximation the degree of dissociation in the test flow is predicted by the stagnation conditions upstream of the secondary diaphragm.

A similar plot for a group of air tests is shown in figure 13. Here the data have been plotted as a function of H_2 because the data trend is not in agreement with the RSFE model. The data fall into two distinct groups – those with the diaphragm opener and those without. When the diaphragm opener was used, the ratio was less than unity and was in good agreement with the ISFE model; however, when the diaphragm opener was not used, the ratio was greater than unity. This result would imply that the mass fraction of O_2 in the test flow was greater than that in the initial test-gas mixture. Similar results were reported in reference 1, and the authors still have no explanation for this effect.

CONCLUDING REMARKS

Simultaneous time-resolved measurements of temperature, density, pitot pressure, and wall pressure in both air and O_2 test gases have been obtained in the Langley pilot model expansion tube. These tests show that nonequilibrium chemical effects are present in the test flow and significantly affect the calculation of the flow condition. These effects must be accounted for from the primary shock since calculations have shown the residence time behind the primary shock is too short to allow the flow to reach equilibrium before entering the expansion fan; measurements have shown that the degree of dissociation in the test gas is determined by conditions upstream of the second diaphragm for some test conditions.

The measured vibrational temperatures were higher than both the equilibrium predictions and the translational temperatures inferred from the measured density and wall pressure. The vibrational temperature showed significant relaxation during the test flow, thereby demonstrating that vibrational nonequilibrium effects were most significant early in the flow.

The use of splitter plates to reduce the boundary-layer effects on the density and temperature measurement showed that the discrepancy between the measured pitot pressure and the value inferred from the measured density and interface velocity was not a result of the measurements being made across the tube boundary layer.

The use of an electromagnetic device to open the secondary diaphragm prior to the arrival of the primary shock resulted in an improvement in the agreement between the measured and inferred pitot pressure. Because of the small numbers of tests with the opener, this result is not conclusive; however, it does indicate that the effects of the opening of the secondary diaphragm may have a strong influence on the test flow.

Langley Research Center
National Aeronautics and Space Administration
Hampton, Va. 23665
October 22, 1975

REFERENCES

1. Haggard, Kenneth V.: Free-Stream Temperature, Density, and Pressure Measurements in an Expansion Tube Flow. NASA TN D-7273, 1973.
2. Jones, Jim J.; and Moore, John A.: Exploratory Study of Performance of the Langley Pilot Model Expansion Tube With a Hydrogen Driver. NASA TN D-3421, 1966.
3. Jones, J. J.: Some Performance Characteristics of the LRC $3\frac{3}{4}$-Inch Pilot Expansion Tube Using an Unheated Hydrogen Driver. Fourth Hypervelocity Techniques Symposium, Univ. of Denver and Arnold Eng. Develop. Center, Nov. 1965, pp. 7-26.
4. Friesen, Wilfred J.: Use of Photoionization in Measuring Velocity Profile of Free-Stream Flow in Langley Pilot Model Expansion Tube. NASA TN D-4936, 1968.
5. Trimpi, Robert L.: A Preliminary Theoretical Study of the Expansion Tube, A New Device for Producing High-Enthalpy Short-Duration Hypersonic Gas Flows. NASA TR R-133, 1962.
6. Trimpi, Robert L.: A Preliminary Study of a New Device for Producing High-Enthalpy, Short-Duration Gas Flows. Advances in Hypervelocity Techniques, Arthur M. Krill, ed., Plenum Press, 1962, pp. 425-451.
7. Weilmuenster, K. James: A Finite-Difference Solution for Unsteady Wave Interactions With an Application to the Expansion Tube. Recent Developments in Shock Tube Research, Daniel Bershader and Wayland Griffith, eds., Stanford Univ. Press, 1973, pp. 534-545.
8. Connor, Laurence Neuman, Jr.: The One-Dimensional Unsteady Expansion of a Reacting Mixture of Gases Considering Vibrational and Chemical Nonequilibrium. Ph. D. Thesis, North Carolina State Univ., 1965.
9. Connor, Laurence N., Jr.; and Taylor, Frances W.: The Centered One-Dimensional Unsteady Expansion of a Vibrationally Relaxing Nitrogen-Oxygen Mixture. NASA TN D-3805, 1967.
10. Connor, Laurence N., Jr.: Calculation of the Centered One-Dimensional Unsteady Expansion of a Reacting Gas Mixture Subject to Vibrational and Chemical Nonequilibrium. NASA TN D-3851, 1967.
11. Moore, John A.: Description and Initial Operating Performance of the Langley 6-Inch Expansion Tube Using Heated Helium Driver Gas. NASA TM X-3240, 1975.
12. Laney, Charles C., Jr.: Microwave Interferometry Technique for Obtaining Gas Interface Velocity Measurements in an Expansion Tube Facility. NASA TM X-72625, 1974.
13. Anderson, Olof L.: A Method for the Measurement of Air Temperature Under Nonequilibrium Conditions. Proceedings of the Fourth Shock Tube Symposium, George D. Teel, compiler, Rep. No. 1160, Ballistic Res. Lab., Feb. 1962, pp. 184-195.

14. Anderson, Olof L.: An Experimental Method for Measuring the Flow Properties of Air Under Equilibrium and Non-Equilibrium Flow Conditions. The High Temperature Aspects of Hypersonic Flow, Wilbur C. Nelson, ed., AGARDograph 68, Pergamon Press, 1964, pp. 299-313.

15. Evans, John S.; and Schexnayder, Charles J., Jr.: An Investigation of the Effect of High Temperature on the Schumann-Runge Ultraviolet Absorption Continuum of Oxygen. NASA TR R-92, 1961.

16. Herzberg, Gerhard: Molecular Spectra and Molecular Structure. I. Spectra of Diatomic Molecules. Second ed., D. Van Nostrand Co., Inc., c.1950. (Reprinted Feb. 1963.)

17. Miller, Charles G., III: A Program for Calculating Expansion-Tube Flow Quantities for Real-Gas Mixtures and Comparison With Experimental Results. NASA TN D-6830, 1972.

18. Bittker, David A.; and Scullin, Vincent J.: General Chemical Kinetics Computer Program for Static and Flow Reactions, With Application to Combustion and Shock-Tube Kinetics. NASA TN D-6586, 1972.

TABLE 1.- TEST CONDITIONS

Run	p_1, Pa	p_{10}, Pa	$V_{S,1}$, m/s	V_i, m/s	Test gas
Diaphragm opener					
3646	2933	26.7	2718	5746	Air
3647	2933	13.3	2942	5499	Air
3648	2933	6.67	2873	5390	Air
3649	2933	2.67	2808	5806	Air
Splitter plates					
3660	2933	40	2855	5034	Air
3661	2933	133	2929	5240	Air
3662	2933	133	2917	4938	Air
3663	2933	133	2779	4961	Air
3664	2933	133	2996	5053	Air
3665	2933	66.7	2872	5667	Air
3666	2933	66.7	2886	5291	Air
3667	2933	40	2878	5451	Air
3668	2933	40	2874	5046	Air
3669	2933	66.7	2911	5083	Air
3670	2933	66.7	2860	4980	Air
3674	2933	26.7	2961	5678	O_2
3675	2933	13.3	2912	5730	O_2
3676	2933	13.3	2955	6101	O_2
3677	2933	13.3	2806	6014	O_2
3678	2933	6.67	2832	6112	O_2
3679	2933	(a)	2865	6247	O_2
3680	2933	(a)	2858	6354	O_2
3683	1467	13.3	3310	6458	O_2
3684	667	13.3	3607	6236	O_2
3685	333	13.3	4002	6212	O_2
3686	1467	13.3	3331	6361	O_2
3687	667	13.3	3767	6347	O_2
3688	333	13.3	3834	6325	O_2
3690	2933	6.67	2957	6003	O_2

[a]Less than 1 Pa.

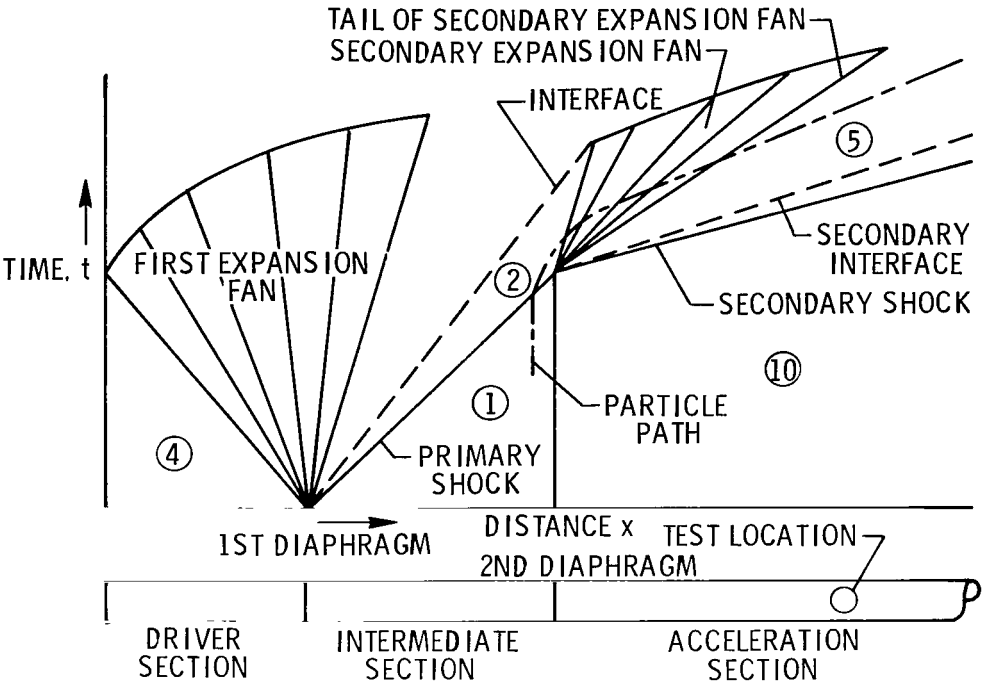

(a) Expansion tube flow cycle showing pertinent flow regions.

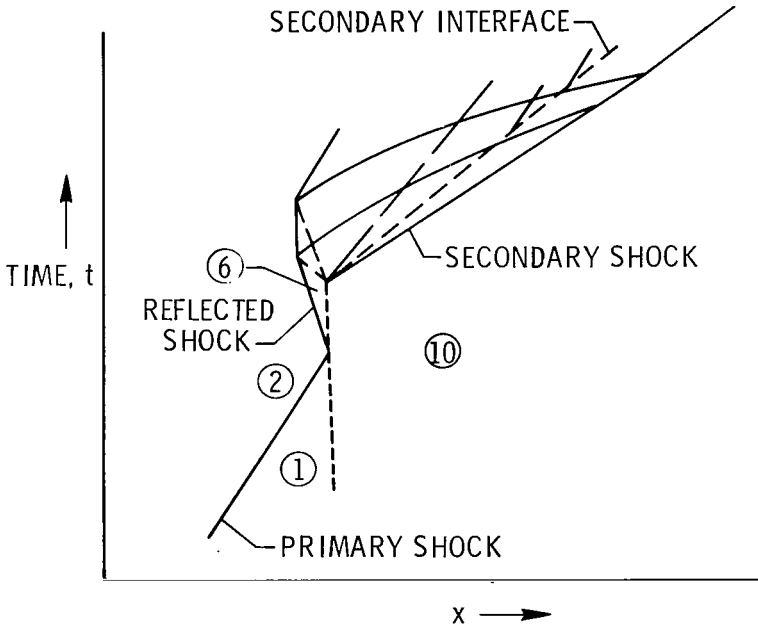

(b) Expansion flow cycle at region of second diaphragm, with effects of diaphragm considered.

Figure 1.- Distance-time diagrams.

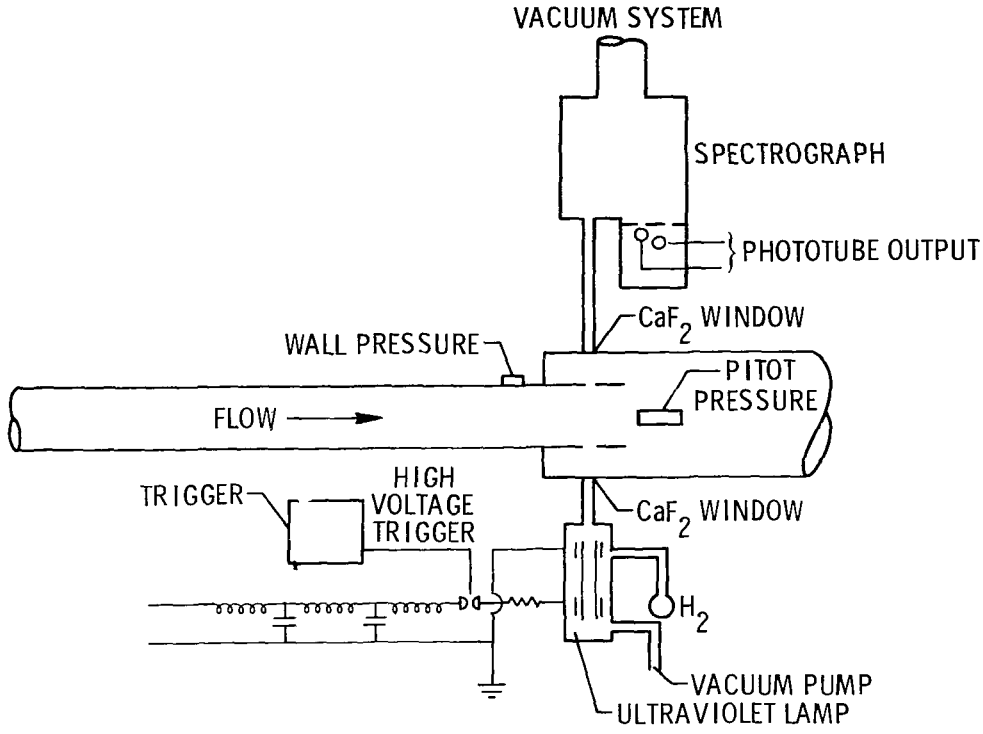

(a) Test section without splitter plates.

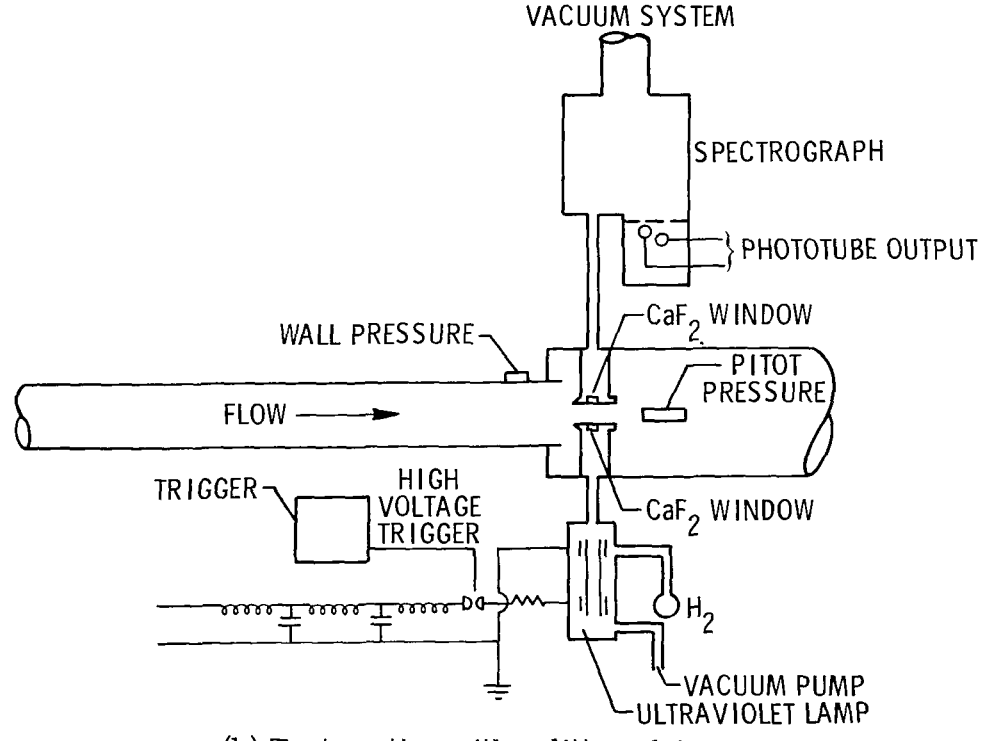

(b) Test section with splitter plates.

Figure 2.- Sketch of test section and lamp assembly.

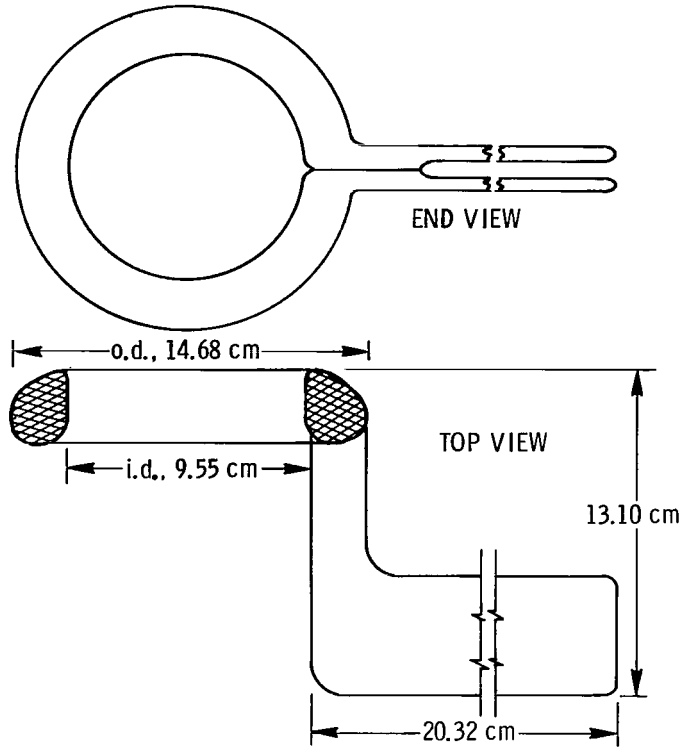

Figure 3.- Diaphragm-opener coil.

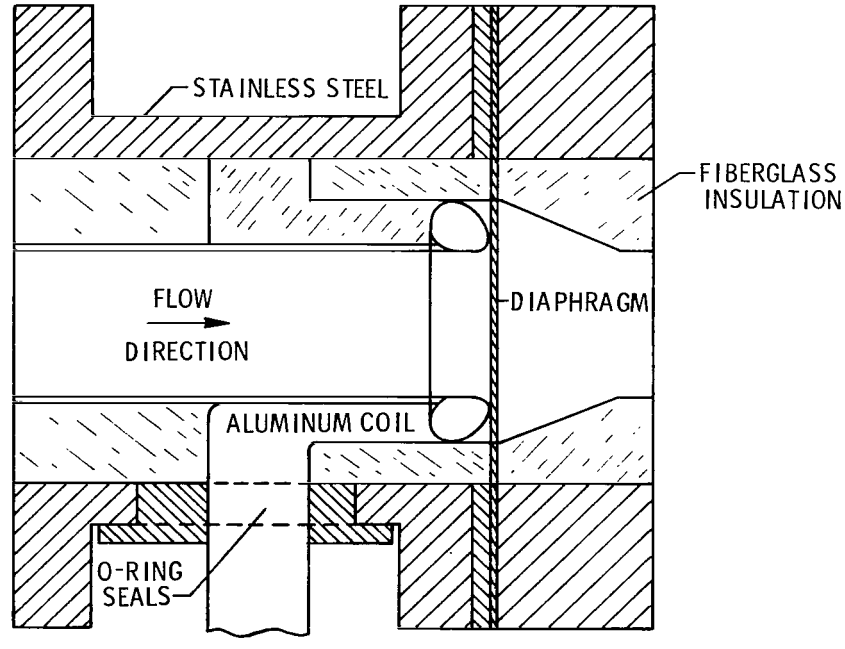

Figure 4.- Installation of coil in expansion tube.

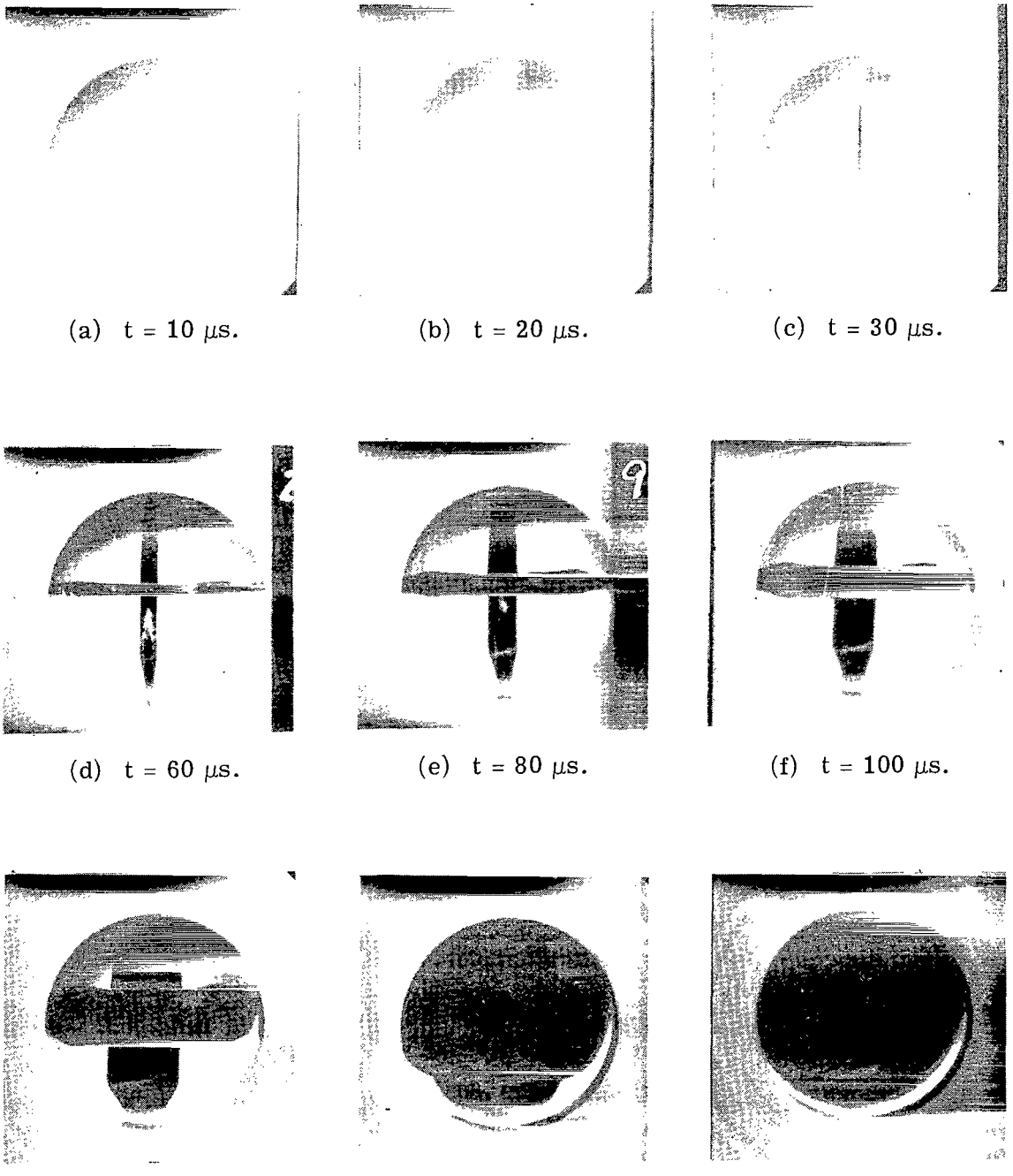

(a) t = 10 μs. (b) t = 20 μs. (c) t = 30 μs.

(d) t = 60 μs. (e) t = 80 μs. (f) t = 100 μs.

(g) t = 140 μs. (h) t = 190 μs. (i) t = 240 μs.

L-75-237

Figure 5.- Diaphragm opening process for intervals of time t after trigger.

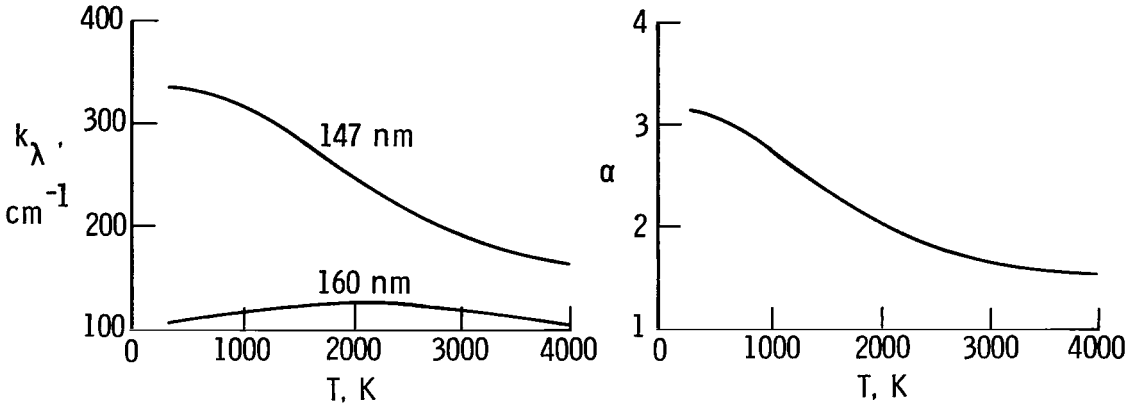

Figure 6.- Temperature dependence of absorption coefficients and their ratio (from ref. 14).

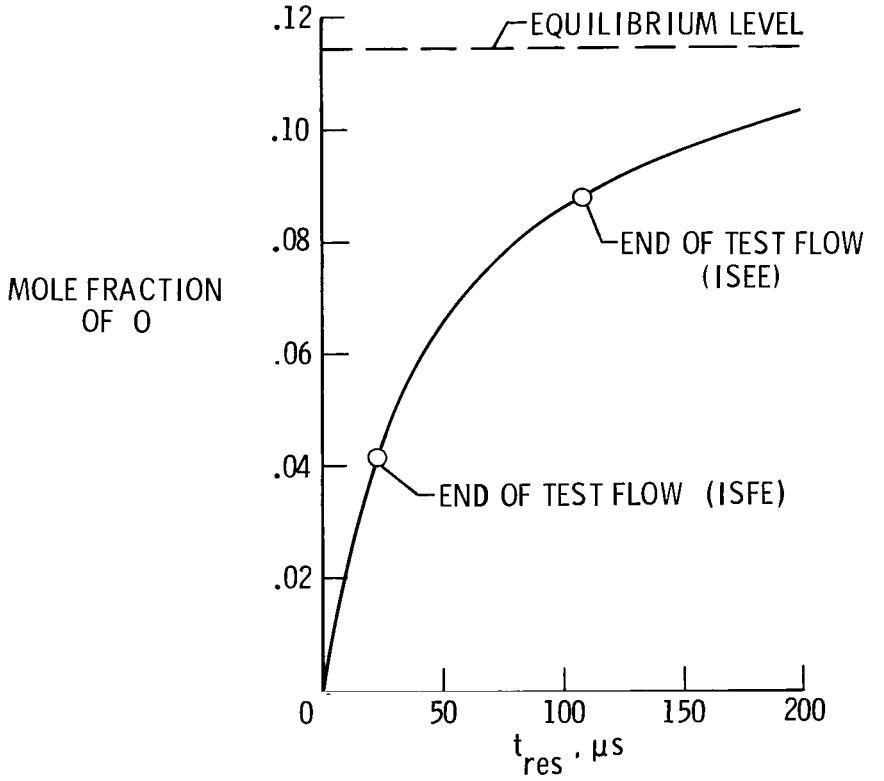

Figure 7.- Mole fraction of O upon entrance into expansion fan. p_1 = 2932 Pa; T_1 = 300 K; $V_{S,1}$ = 2956 m/s; test gas: O_2.

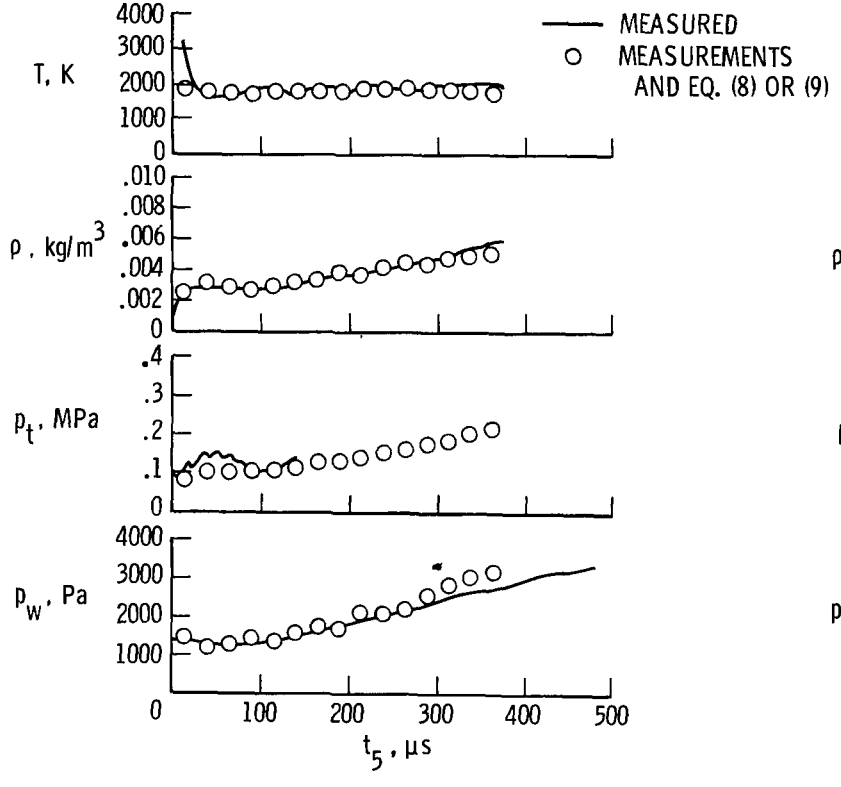

Figure 8.- Measured and inferred flow quantities for run 3676 of table 1. p_1 = 2933 Pa; T_1 = 300 K; $V_{S,1}$ = 2955 m/s; V_i = 6101 m/s; test gas: O_2.

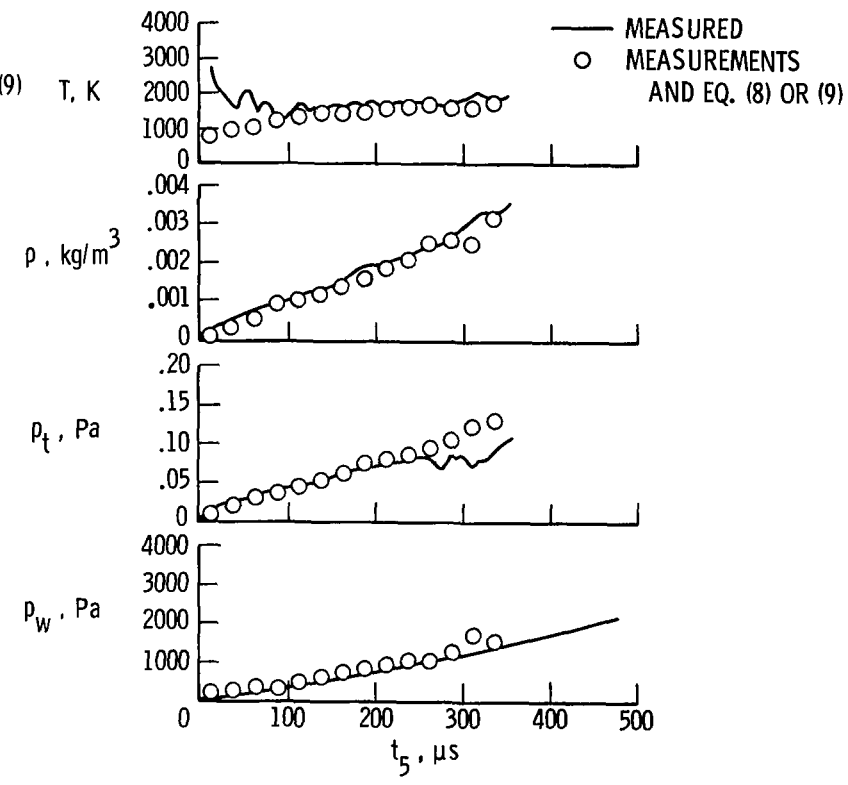

Figure 9.- Measured and inferred flow quantities for run 3679 of table 1. p_1 = 2933 Pa; T_1 = 300 K; $V_{S,1}$ = 2865 m/s; V_i = 6247 m/s; test gas: O_2.

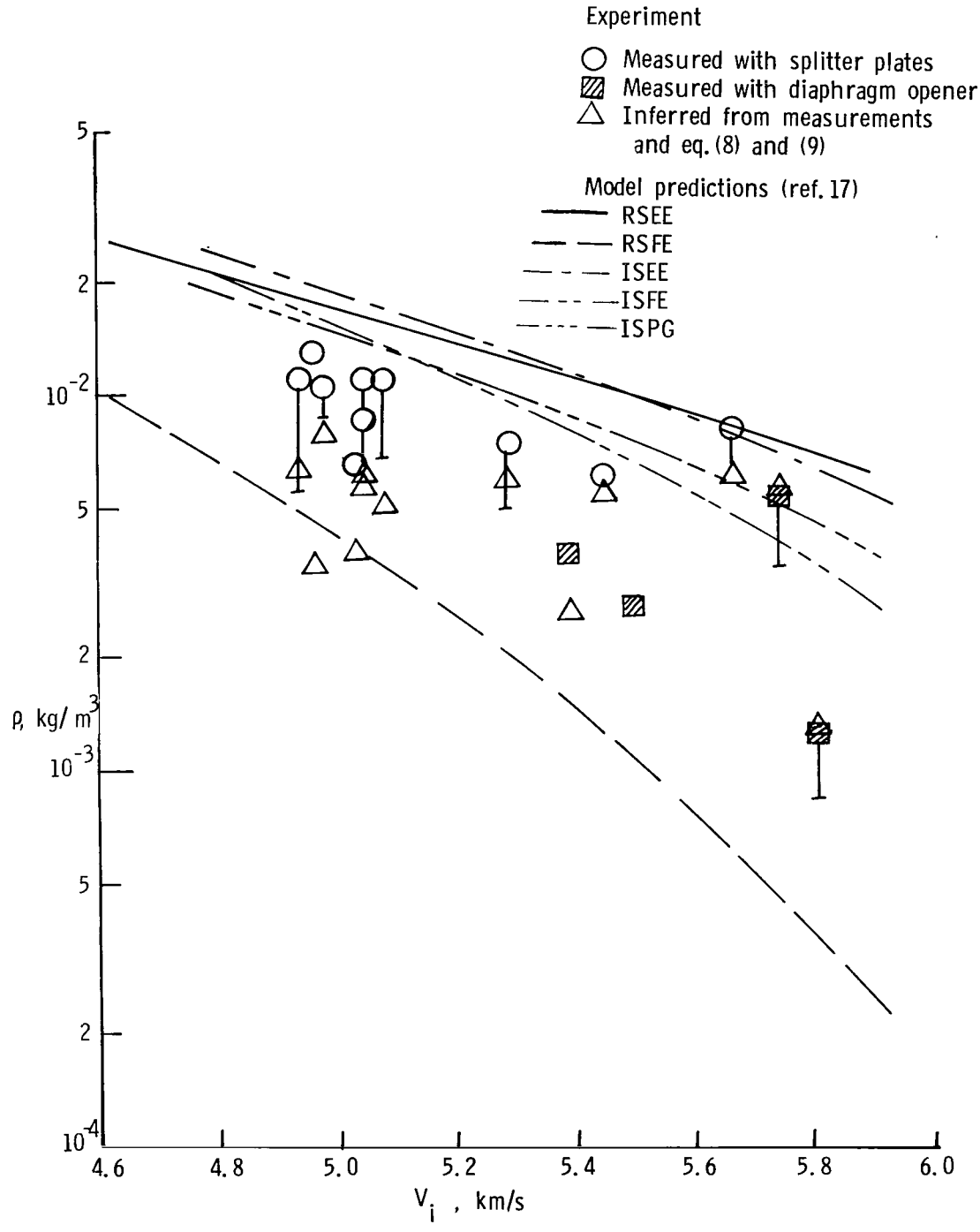

(a) Density.

Figure 10.- Comparison of measured, inferred, and predicted test data for air test gas. $V_{S,1}$ = 2880 m/s; p_1 = 2932 Pa; T_1 = 300 K.

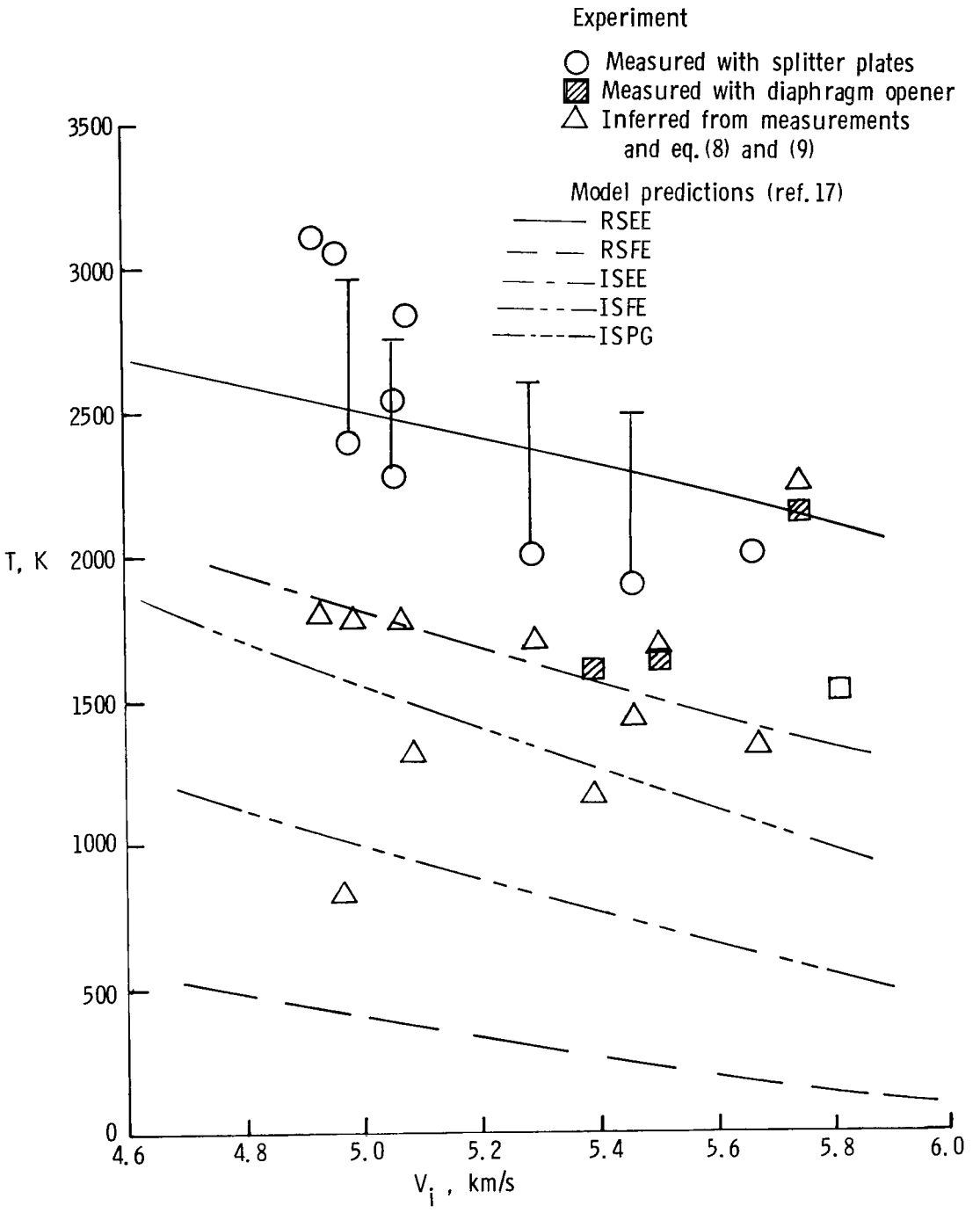

(b) Temperature.

Figure 10.- Continued.

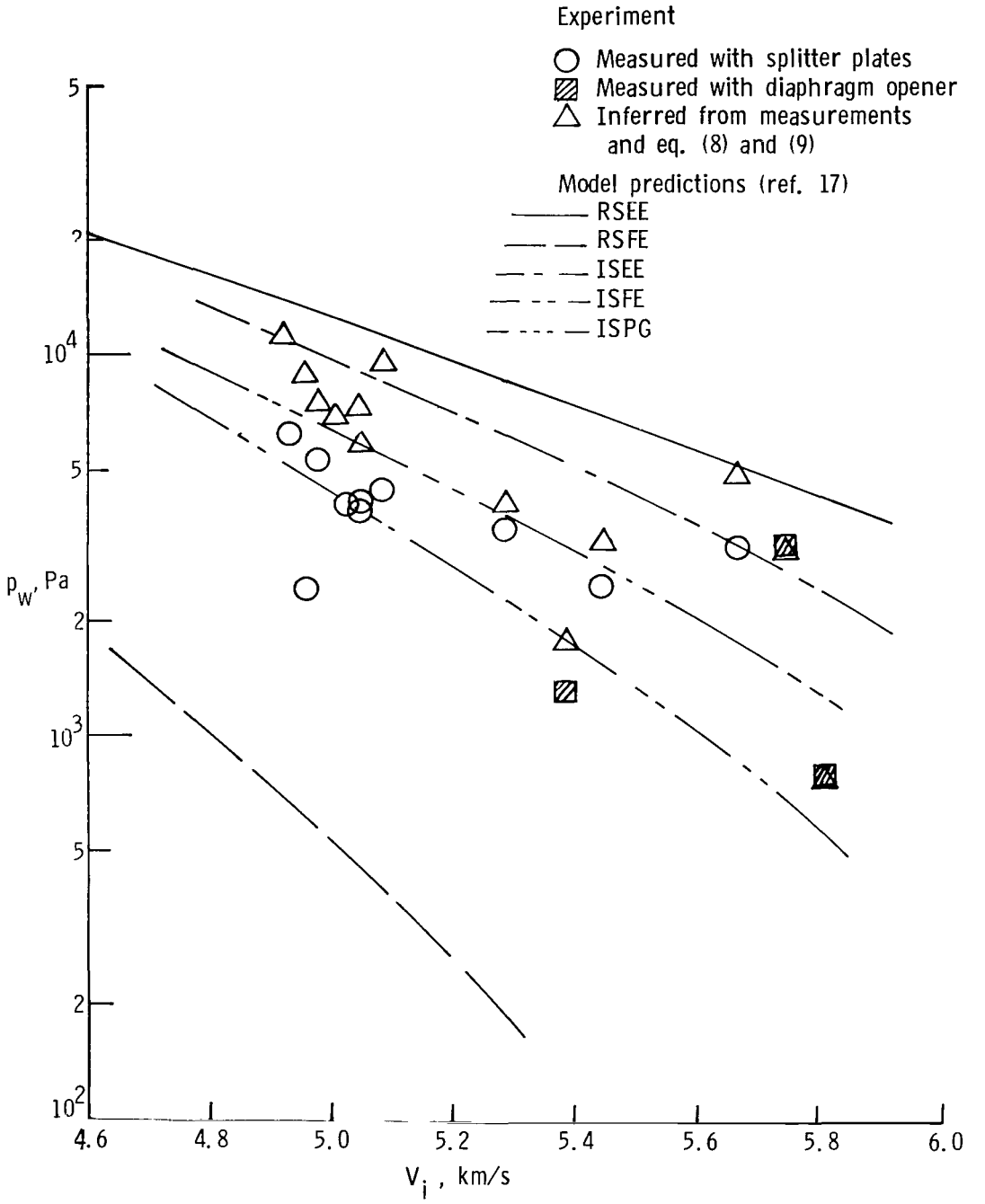

(c) Wall pressure.

Figure 10.- Continued.

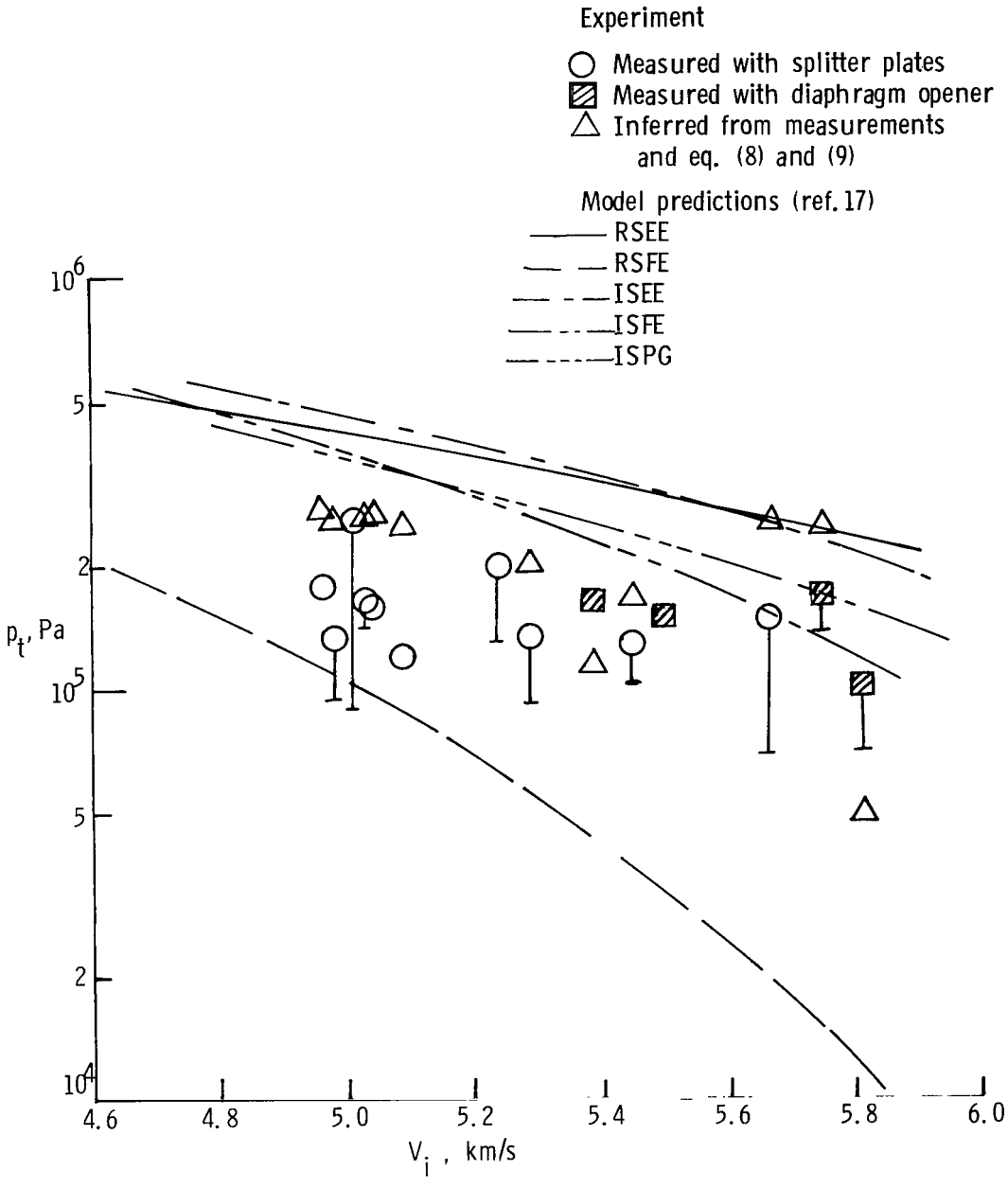

(d) Pitot pressure.

Figure 10.- Concluded.

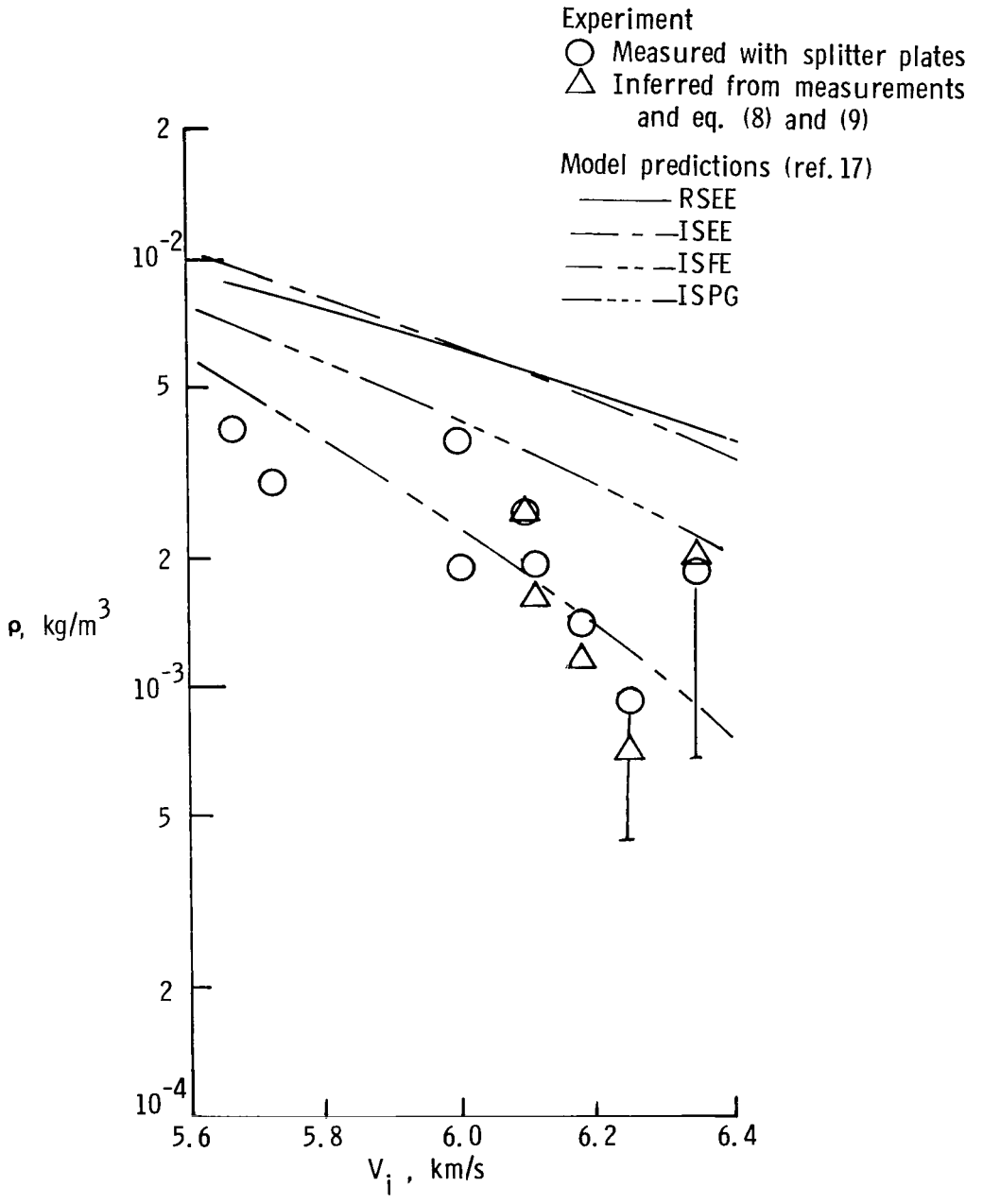

(a) Density.

Figure 11.- Comparison of measured, inferred, and predicted test data for O_2 test gas. $V_{S,1}$ = 2906 m/s; p_1 = 2932 Pa; T_1 = 300 K.

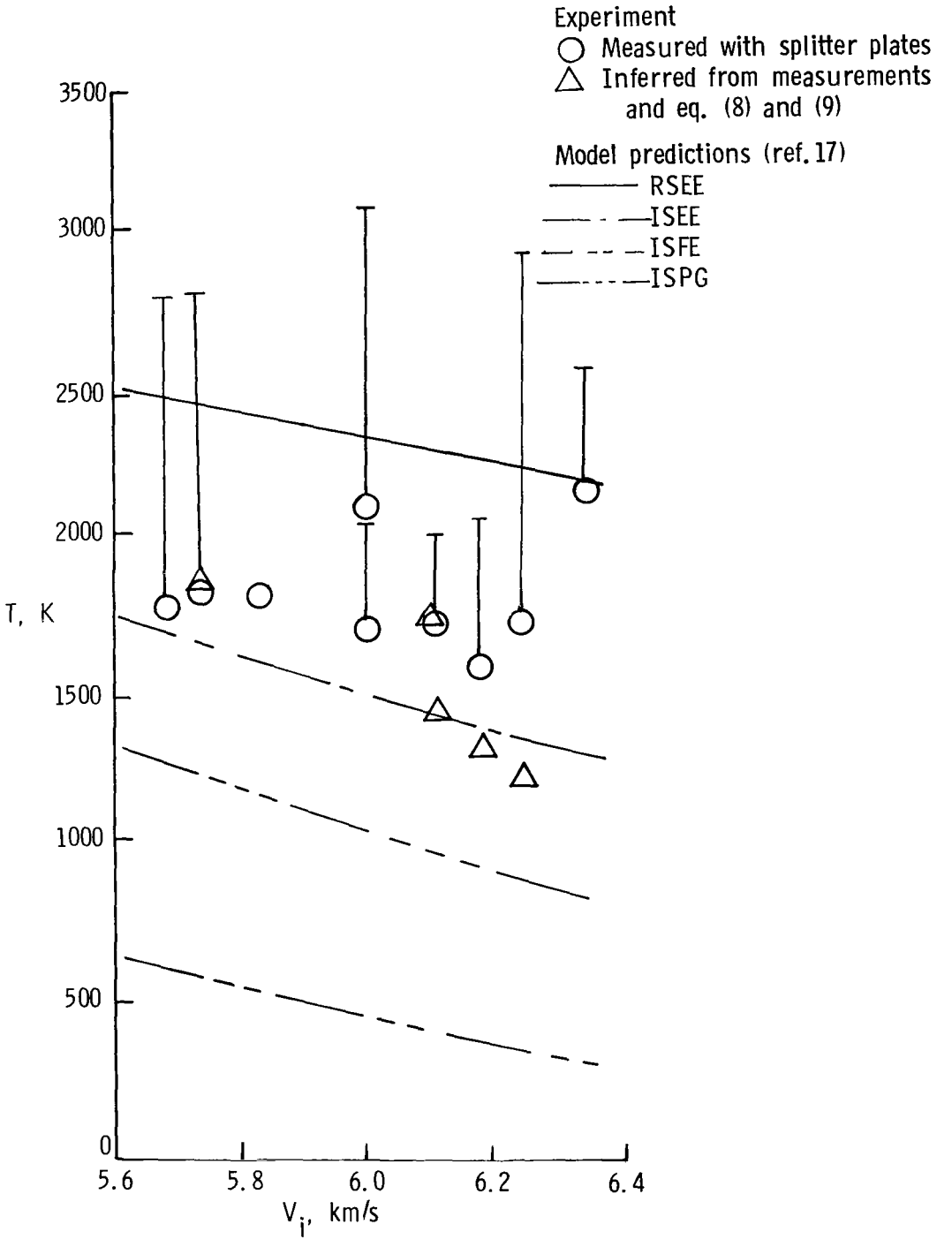

(b) Temperature.

Figure 11.- Continued.

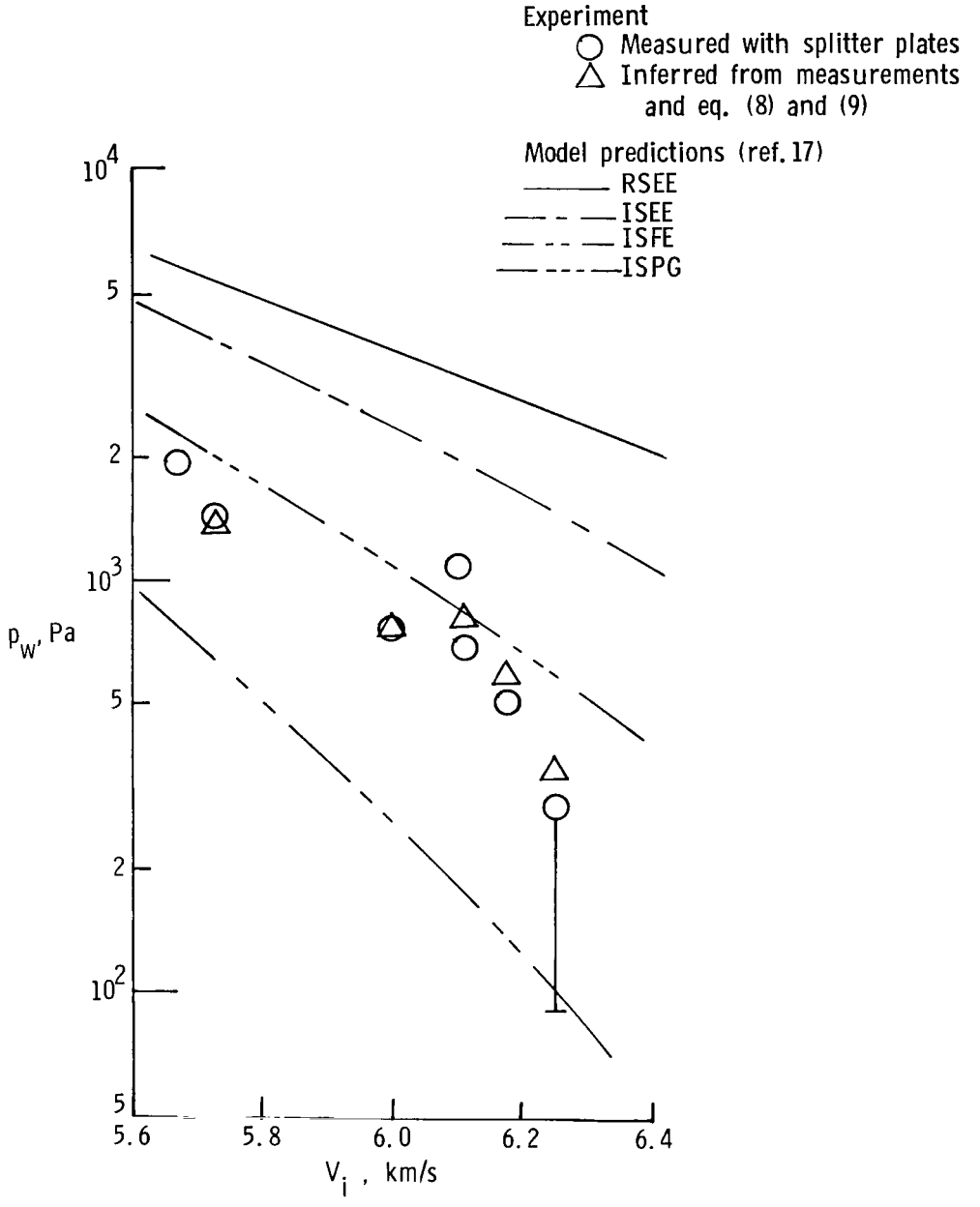

(c) Wall pressure.

Figure 11.- Continued.

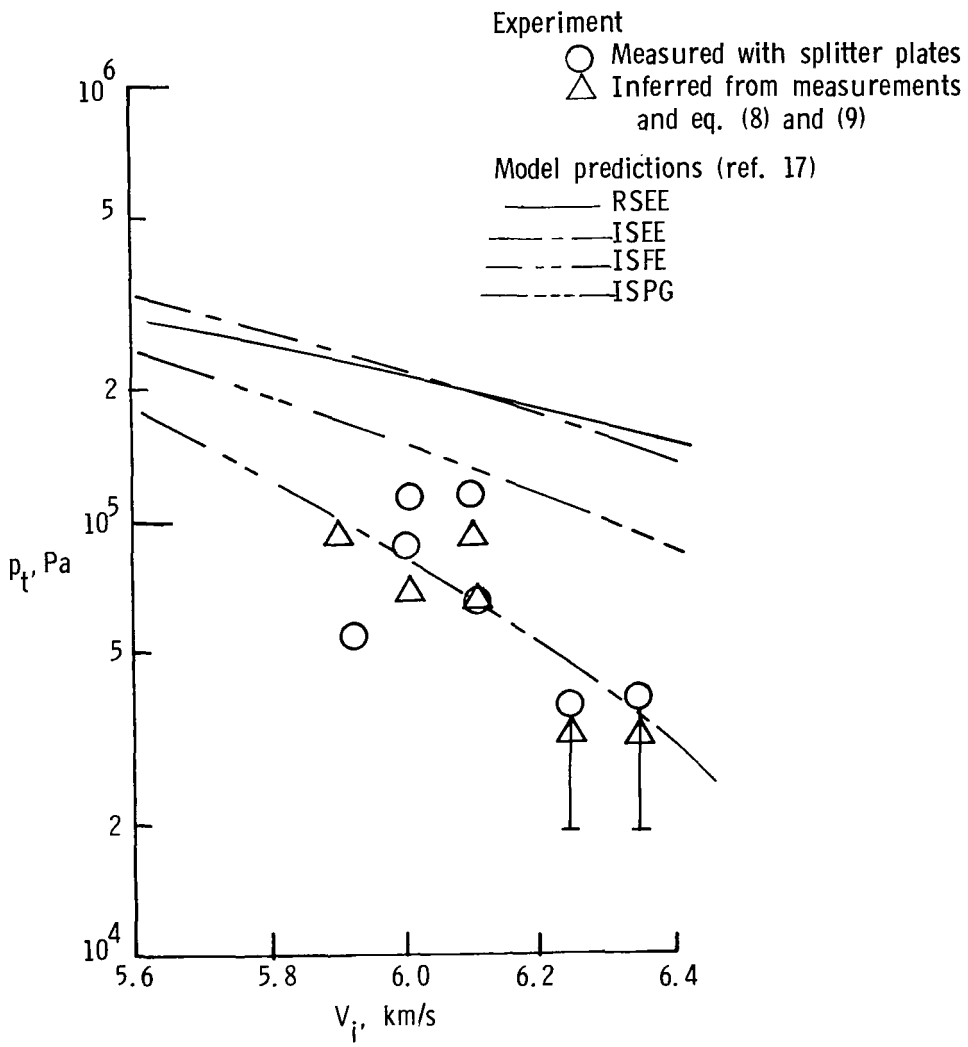

(d) Pitot pressure.

Figure 11.- Concluded.

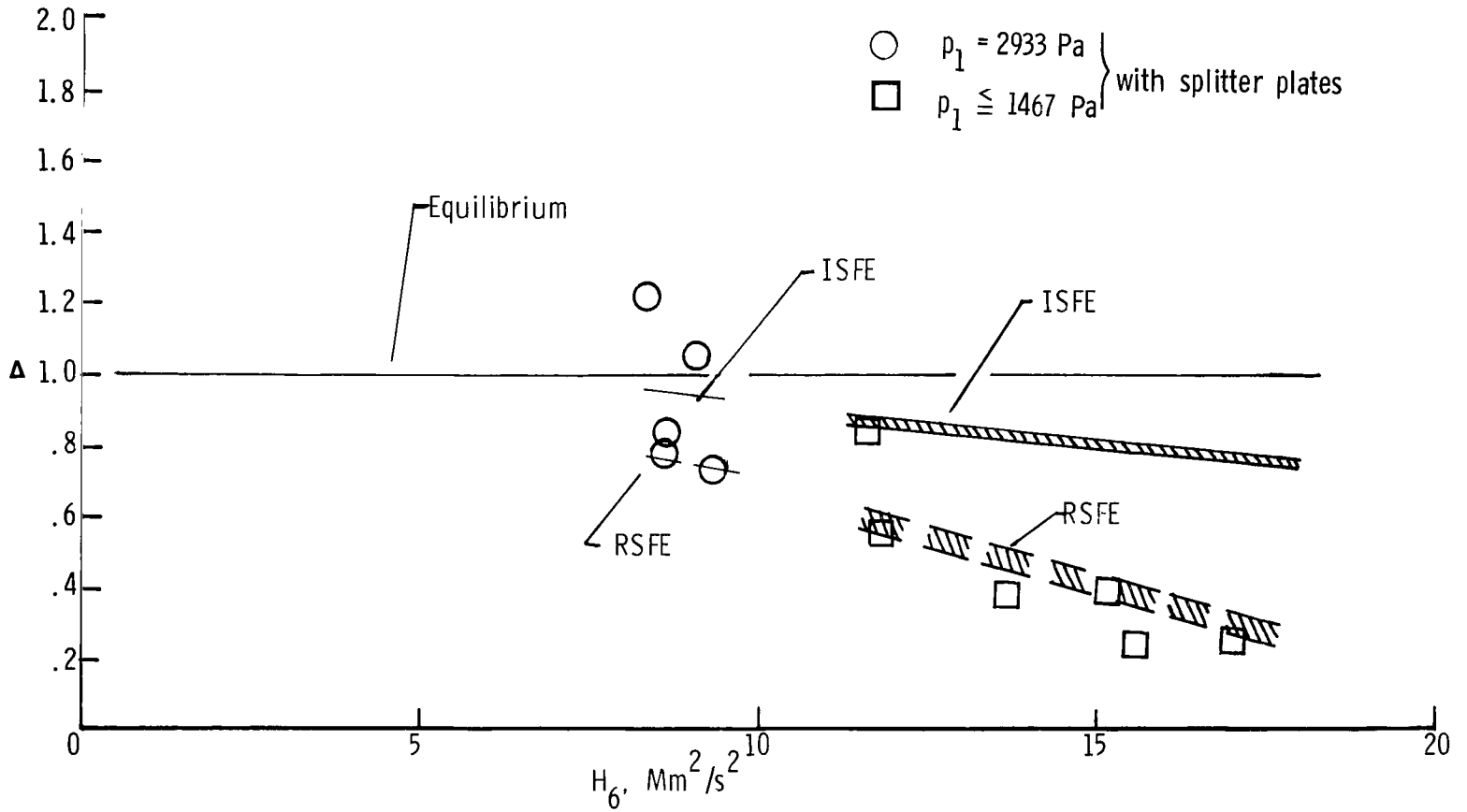

Figure 12.- Variation of Δ with H_6 for O_2 test gas. T_1 = 300 K.

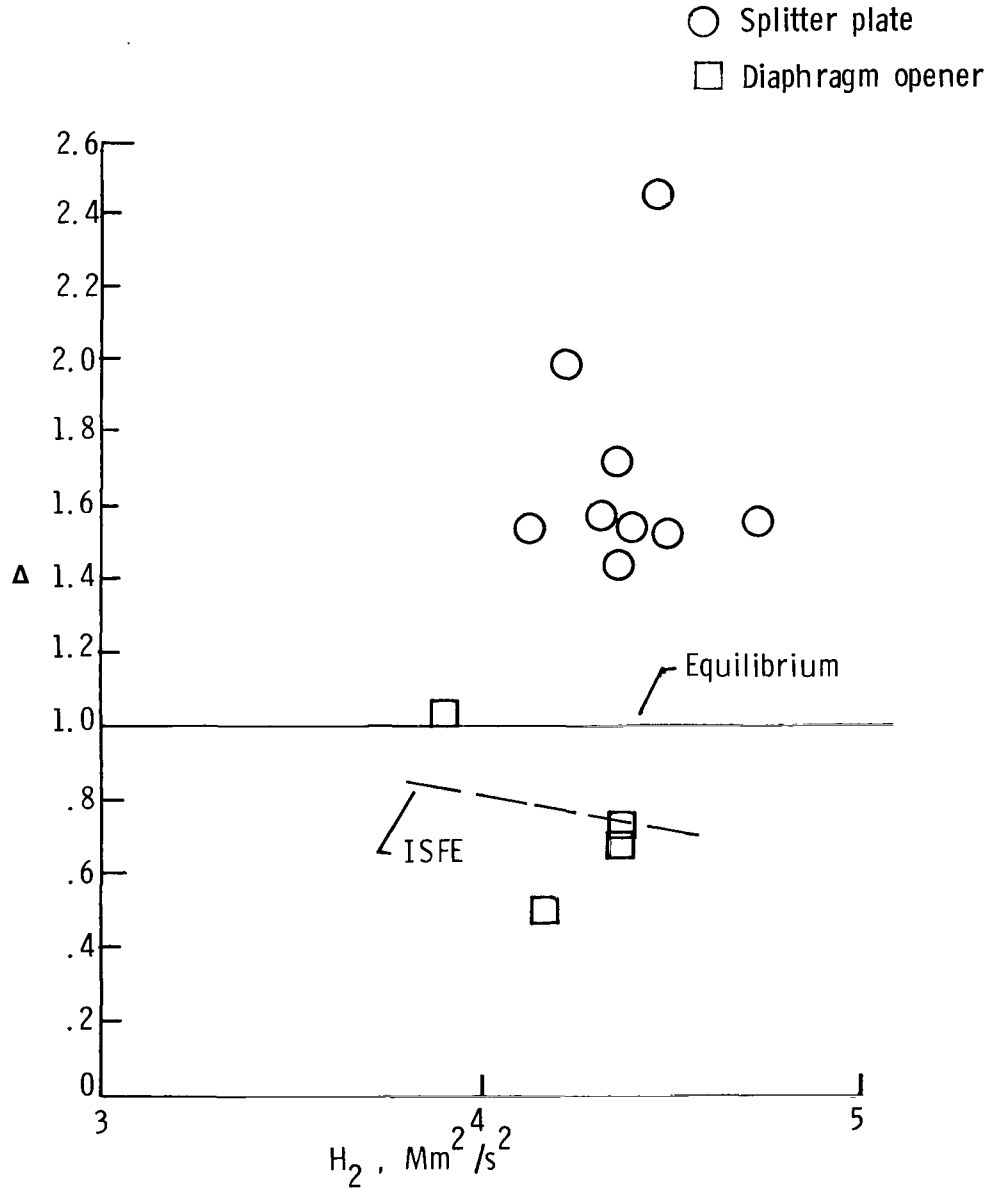

Figure 13.- Variation of Δ with H_2 for air test gas.
p_1 = 2933 Pa; T_1 = 300 K.

NASA-Langley, 1975 L-10356

"The aeronautical and space activities of the United States shall be conducted so as to contribute . . . to the expansion of human knowledge of phenomena in the atmosphere and space. The Administration shall provide for the widest practicable and appropriate dissemination of information concerning its activities and the results thereof."

—NATIONAL AERONAUTICS AND SPACE ACT OF 1958

NASA SCIENTIFIC AND TECHNICAL PUBLICATIONS

TECHNICAL REPORTS: Scientific and technical information considered important, complete, and a lasting contribution to existing knowledge.

TECHNICAL NOTES: Information less broad in scope but nevertheless of importance as a contribution to existing knowledge.

TECHNICAL MEMORANDUMS: Information receiving limited distribution because of preliminary data, security classification, or other reasons. Also includes conference proceedings with either limited or unlimited distribution.

CONTRACTOR REPORTS: Scientific and technical information generated under a NASA contract or grant and considered an important contribution to existing knowledge.

TECHNICAL TRANSLATIONS: Information published in a foreign language considered to merit NASA distribution in English.

SPECIAL PUBLICATIONS: Information derived from or of value to NASA activities. Publications include final reports of major projects, monographs, data compilations, handbooks, sourcebooks, and special bibliographies.

TECHNOLOGY UTILIZATION PUBLICATIONS: Information on technology used by NASA that may be of particular interest in commercial and other non-aerospace applications. Publications include Tech Briefs, Technology Utilization Reports and Technology Surveys.

Details on the availability of these publications may be obtained from:

SCIENTIFIC AND TECHNICAL INFORMATION OFFICE

NATIONAL AERONAUTICS AND SPACE ADMINISTRATION

Washington, D.C. 20546